Visualization of the Barkhausen Effect by Magnetic Force Microscopy

Alexander Schwarz,* Marcus Liebmann,† Uwe Kaiser, and Roland Wiesendanger
Institute of Applied Physics, University of Hamburg, Jungiusstrasse 11, 20355 Hamburg, Germany

Tae Won Noh and Dong Wook Kim‡
School of Physics & ReCOE, Seoul National University, Seoul, 151-747, South Korea
(Received 18 August 2003; published 20 February 2004)

By visualization of the Barkhausen effect using magnetic force microscopy we are able to provide detailed information about the physical principles that govern the magnetization reversal of a granular ferromagnetic thin film with perpendicular anisotropy. Individual Barkhausen volumes are localized and distinguished as either newly nucleated or grown by domain wall propagation. The Gaussian size distribution of nucleated Barkhausen volumes indicates an uncorrelated random process, while grown Barkhausen volumes exhibit an inverse power law distribution, which points towards a critical behavior during domain wall motion.

DOI: 10.1103/PhysRevLett.92.077206 PACS numbers: 75.60.Ej, 75.60.Jk, 75.70.Ak

The magnetization reversal of ferromagnets is a rather complex but technological important phenomenon. Macroscopically, it is characterized by the hysteresis loop, which is composed of a series of discrete magnetization jumps, known as the Barkhausen effect [1]. Thorough examination of such individual events provides information about fundamental mechanisms of the reversal processes themselves, i.e., domain nucleation or domain wall propagation, which are related to magnetic as well as to structural properties. Detection of individual Barkhausen jumps on the nanometer scale in granular, and thereby disordered, thin films is very demanding and of particular interest due to its impact on the magnetic recording technology [2]. In such films, grain boundaries provide pinning sites, which impede domain wall motion and thus enable magnetic information storage. Since areal bit densities in today's longitudinal media with in-plane magnetization rapidly approach the superparamagnetic limit [3], thin films with perpendicular anisotropy are currently investigated intensively, because a significantly higher maximum packing density has been predicted for them [4].

Our sample, an 80 nm thick $La_{0.7}Sr_{0.3}MnO_3$ film, was epitaxially grown on a $LaAlO_3(001)$ substrate by pulsed laser deposition. This material belongs to the class of mixed valence manganites, which recently attracted a lot of interest due to its colossal magneto-resistive effect [5]. Its granular nanocrystalline structure is typical for technological relevant thin films [2]. Because of a small lattice mismatch, the film is compressed in-plane and elongated in the normal direction, which induces a uniaxial perpendicular anisotropy [6,7]. Dislocation lines, 20–40 nm apart, compensate for most of the in-plane stress and are responsible for the structural disorder in the material. Above 70 nm thickness, the dislocation network develops into orthogonal shaped columns with amorphous grain boundaries [8]. Consistent with these studies on the internal film structure are scanning force microscopy (SFM) images of our samples, which show a granular surface topography with a mean diameter around 32 nm and a root-mean-square roughness of 0.4 nm.

To visualize individual Barkhausen jumps we employed magnetic force microscopy (MFM) using our home-built ultrahigh vacuum low temperature force microscope (Hamburg design) [9]. After saturating the sample at 5.2 K in a perpendicular magnetic field of 600 mT, the field was ramped quasistatically from remanence towards saturation and back again along the major hysteresis loop, while continuously recording MFM images [10]. Because of our preparation technique [9], the nominally 5 nm thick iron film is evaporated only on that

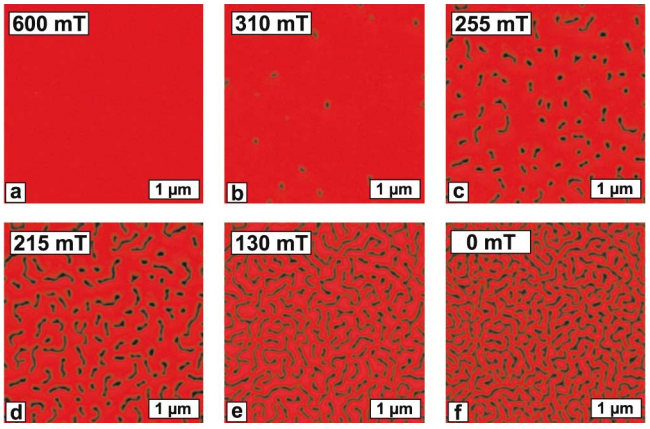

FIG. 1 (color). Domain structures of the $La_{0.7}Sr_{0.3}MnO_3$ thin film recorded along the decreasing branch of the major hysteresis loop. (a)–(f) are part of a series consisting of 158 images [10], which have been acquired on the same scan area while slowly ramping the magnetic field (5 or 10 mT/image). Image parameters (see Ref. [10] for their explanation): Tip coating: 5 nm Fe, scan height $h = 24$ nm, $f_0 = 195$ kHz, $c_z = 47$ N/m, $A_0 = \pm 5$ nm, $U_{\text{bias}} = -0.1$ V, Δf-range $= 0.7$ Hz.

side face of the pyramidal tip, which is oriented (within a few degrees) perpendicular to the surface, i.e., parallel to the external field. Therefore, the tip interacts even in large external fields nearly exclusively with the out-of-plane component of the sample stray field.

Figure 1 displays six exemplary MFM images recorded on the decreasing branch of the hysteresis loop. Bright and dark regions correspond to attractive and repulsive magnetostatic interactions between the gradient of the tip stray field and the magnetic poles at the surface [11]. In saturation [Fig. 1(a)], the contrast is homogeneous. At 310 mT [Fig. 1(b)], several circular domains are already nucleated. After reducing the field further [Figs. 1(c)–1(e)], the domains become elongated. In remanence [Fig. 1(f)], about 44.7% (7.152 μm^2) of the scan range (16 μm^2) reversed their polarization. A maze type pattern with a mean domain width of 79 nm has evolved, in accordance with previous measurements [12].

To examine individual Barkhausen jumps a procedure illustrated in Fig. 2 has been applied to the whole image series. Two consecutive images [cf., Figs. 2(a) and 2(b)] are subtracted from each other. The resulting difference image [Fig. 2(c)] then includes only reversed areas. Each white region represents the size and position of one individual Barkhausen jump. To distinguish between domain nucleation and growth by wall propagation, the difference images can be merged into the original domain pattern as demonstrated in Fig. 2(d). Newly nucleated domains are identified as isolated regions (N), while grown regions are connected to already existing domains (G).

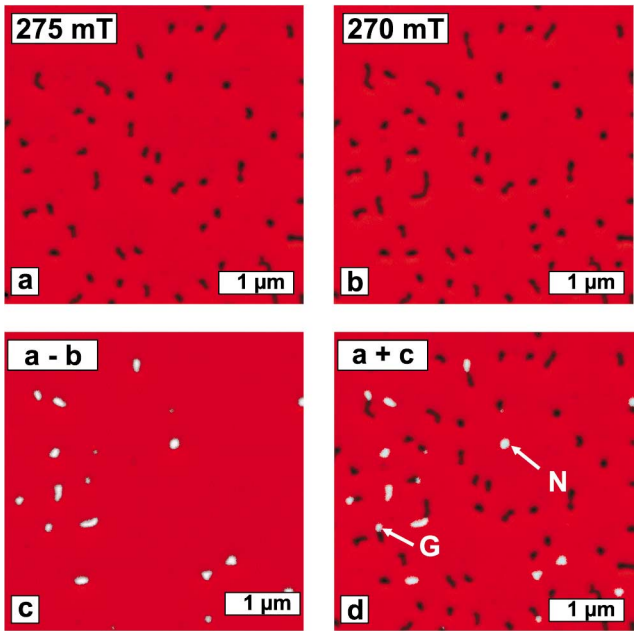

FIG. 2 (color). Visualization and localization of individual Barkhausen jumps from consecutive MFM images. (a) and (b) have been recorded from 275–270 mT and 270–265 mT, respectively. The difference image (c) = (a)–(b) visualizes the reversed regions. In the merged image (d) = (a) + (c), their positions with respect to the initial domain pattern can be determined. The arrows indicate examples for an isolated nucleated Barkhausen volume (N) and a Barkhausen volume adjacent to an already existing domain that has been grown by wall propagation (G).

In a first approximation, the size of each reversed area in difference images such as Fig. 2(c) can be obtained by counting all connected pixels just above the noise level of the experimental data. Since thin films are two-dimensional systems, the volume V_B of each Barkhausen jump can be computed via $V_B = a_B \cdot t = \pi r_B^2 \cdot t$, where t is the film thickness and r_B is the radius corresponding to the reversed area a_B. However, for a thorough analysis, it has to be considered that areas measured in this way are not the *true* reversed areas, but a convolution of the magnetic poles at the surface with the gradient of the tip stray field. As a consequence, the sum of all areas in our difference images from saturation to remanence is more than 5 times larger than the totally reversed area of 7.152 μm^2. Since domain widths in quasiperiodic structures are reproduced correctly, this quantity can be accurately determined from the remanent domain pattern in Fig. 1(f). To determine a more precise value of the reversed areas, the integral of the corresponding contrast (in units of Hz $\cdot$ nm^2) is additionally extracted from the data set [13]. This quantity is proportional to the magnetic pole density at the surface of the reversed region [14] and therefore a good measure for the true reversed volume. With the side condition that the sum of all contrast integrals between saturation and remanence has to be equal to the totally reversed area of 7.152 μm^2, the true size of each reversed area can be obtained.

After such an analysis, the size distribution of newly nucleated and grown Barkhausen volumes can be plotted. In Fig. 3 this has been done for the radius r_B(N) of nucleated Barkhausen volumes (a) and for grown areas a_B(G) due to domain wall propagation (b). The average size of reversed areas during growth is much smaller than during nucleation (3 020 nm^2 and 16 741 nm^2, respectively). Both processes are accompanied by an energy barrier, pinning, and wall energy, respectively. In order to make an individual reversal event probable, this barrier has to be compensated by an at least equal amount of magnetostatic energy gain. Conclusively, the energy barrier is larger in the case of nucleation. Furthermore, the two size distributions in Fig. 3 look very different, indicating that initial nucleation and subsequent growth of domains are linked to different mechanisms.

The Gaussian size distribution found for r_B(N) [Fig. 3(a)] can be explained as follows. Because of thermal fluctuations, the magnetic moments probe their local energy landscape, which is altered by the external field. The energy balance for thermally activated nucleation is determined by the gain of magnetostatic stray field energy, E_S, the cost of magnetostatic energy in an opposite

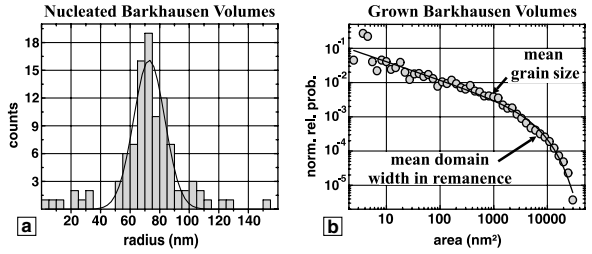

FIG. 3. (a) Size distribution for the radii $r_B(N)$ of nucleated Barkhausen volumes. The solid line is a Gaussian fit with a mean value of 73 nm and width of about 10 nm. (b) Size distribution for the areas $a_B(G)$ of Barkhausen volumes grown by wall propagation using logarithmic binning in a double-logarithmic representation. The solid line corresponds to an inverse power law fit with a critical exponent of $\tau = 0.54$ and a cutoff area $a_0 = 6630\ \mathrm{nm}^2$.

external field (Zeeman energy), E_Z, and the domain wall energy, E_W. For a cylindrical domain E_S and E_Z are proportional to the volume, i.e., $E_S - E_Z \propto r_B^2$, while E_W is proportional to the wall area, i.e., $E_W \propto r_B$. If a surface and volume energy term is present, thermodynamics predicts that only those compact fluctuations remain stable which exceed a certain critical radius. Energy minimization yields $r_c = \mu_0 \gamma / 2J_S(J_S - B) \approx 54$ nm. Here, $J_S = 300$ mT is the saturation magnetization of our sample, $B = 270$ mT is the external magnetic flux density, where we found the largest nucleation rate, and $\gamma = 4(AK_u)^{1/2}$ is the specific wall energy. The latter is determined from $K_u = 20\,000\ \mathrm{Jm}^{-3}$, the magnetocrystalline uniaxial anisotropy coefficient [12] and $A \approx 1.73 \times 10^{-12}\ \mathrm{Jm}^{-1}$, the exchange stiffness constant [15]. This simple estimation is in reasonable good agreement with the experimentally found mean radius of $r_m = 73$ nm. Structural properties did not enter the calculation and indeed the mean size of the nucleated domains is much larger than the mean grain size. However, since we found that the first few newly nucleated domains appear always at nearly identical locations, certain favorable nucleation centers must exist. The observed Gaussian distribution around r_m is a sign of uncorrelated random fluctuations, probably due to imperfections and inhomogeneities that locally alter K_u or A.

The size distribution of grown areas a_B(G) [Fig. 3(b)] is conspicuously different. It follows an inverse power law over three decades, but decreases much quicker beyond a certain cutoff size. The fit for a_B(G) has been done according to $P(a_B) \propto a_B^{-\tau} e^{-a_B/a_0}$, where $\tau = 0.54 \pm 0.03$ is the critical exponent and $a_0 = (6630 \pm 550)\ \mathrm{nm}^2$ is the characteristic cutoff size. Inverse power laws are observed in physical systems at criticality, while in thermal equilibrium an exponential decay of the size distribution is expected. For externally driven systems far from equilibrium the concept of self-organized criticality (SOC) has been introduced [16] and applied to various phenomena [17] including the Barkhausen effect [18]. Such systems organize themselves in a barely stable state, where the dynamics takes place in avalanches. In ferromagnets, the driving force is the magnetic field and a Barkhausen jump corresponds to an avalanche. Whether the Barkhausen effect can be described within the framework of SOC has been discussed controversially [19]. In a phenomenological approach, power law distributions with an exponential cutoff have been found by analyzing the movement of a domain wall through a disordered medium [20]. Any observed scaling in this picture is a consequence of correlations in the pinning potential due to structural defects. Little fluctuations result in a small τ, emphasizing the exponential behavior. Recently, the predicted critical exponent of $\tau = 4/3$ for a single domain wall moving in a disordered two-dimensional system [21] has been experimentally confirmed for a thin film with in-plane magnetization [22]. However, this model is not applicable to our situation, because interactions between domain walls are neglected.

It has been pointed out that the amount of disorder [22,23], as well as the presence of long-range dipolar interactions [24], plays an important role to the understanding of the origin of criticality in the Barkhausen effect. The latter is known to be crucial for domain formation. Its influence is evident in the decreasing mean size of reversed areas per field interval by a factor of 4 upon approaching remanence, because large avalanches become more and more unlikely as the domain pattern converges to its demagnetized state. It is this demagnetization effect that is responsible for the mean domain width of the quasiperiodic maze pattern in remanence and not the mean diameter of nucleated domains, which is nearly twice as large. Moreover, after initial nucleation the hysteresis loop for our sample runs linear from saturation towards remanence [10]. This means that during growth the effective field in the sample (external field reduced by the sample magnetization) is kept constant by the long-range dipolar interaction and the resulting appropriate Barkhausen jumps. As a consequence, domain walls stay always close to the depinning transition. Note, that this type of feedback is consistent with SOC. However, it has been argued that a ferromagnetic system exhibits critical behavior only, if the characteristic length scale of the structural disorder ξ and the magnetic exchange length $l_{ex} \gg (A/K_u)^{1/2}$ are on the same order of magnitude [23]. This kind of fine-tuning contradicts the SOC concept. For our sample, ξ can be identified with the mean grain size of about 32 nm, which is indeed close to $l_{ex} \approx 10$ nm.

Another issue is the origin of the exponential cutoff. In computer simulations, the cutoff in SOC distributions has been attributed to the finite size of the system under investigation, i.e., avalanches cannot become larger than the sample itself [25]. Obviously, the situation is different in our case, because the observed Barkhausen jumps are much smaller than the scan range. The exponential cutoff can be explained either by the nanocrystalline grain structure of the film or by the demagnetization effect.

The latter is supported by the diameters of the largest reversed areas, which are on the order of the domain width in remanence as indicated in Fig. 3(b). In other words, the maximum avalanche size is limited by the long-range magnetostatic interaction. On the other hand, structural defects, like dislocation lines and grain boundaries, provide pinning sites for the domain walls. Since the probability to overcome a certain number of barriers decreases exponentially, reversal processes larger than the typical grain size become considerably more unlikely. Indeed, the size of the areas, where the exponential tail starts, is approximately on the order of the grain size [see Fig. 3(b)].

Concerning the two relevant magnetization processes we can conclude that they obey different physical principles. The Gaussian size distribution during nucleation is a clear sign for an uncorrelated random process. On the other hand, the power law size distribution during growth indicates that the system is kept at criticality during domain wall movement due to the influence of the demagnetizing field. However, since the characteristic structural and magnetic length scales are of similar magnitude, this is not achieved by self-organization in a strict sense.

We would like to thank U. H. Pi and Z. G. Khim. This work is supported by the Deutsche Forschungsgemeinschaft (Grant No. Wi1277/18-1 and Graduiertenkolleg "Physik nanostrukturierter Festkörper").

*To whom correspondence should be addressed.
Email address: aschwarz@physnet.uni-hamburg.de
†Present address: Department of Mechanical Engineering, Yale University, 15 Prospect Street, New Haven, CT 06511, USA.
‡Present address: Samsung Advanced Institute of Technology, Suwon 440-600, South Korea.

[1] H. Barkhausen, Z. Phys. **20**, 401 (1919).
[2] H. N. Bertram and J. G. Zhu, in *Fundamental Magnetization Processes in Thin-Film Recording Media*, Solid State Physics Vol. 46, edited by H. Ehrenreich and D. Turnbull (Academic Press, Boston, 1992).
[3] S. H. Charap, P. L. Lu, and Y. He, IEEE Trans. Magn. **33**, 978 (1997).
[4] For a review on perpendicular recording, see, e.g., W. Andrä, H. Danan, and R. Mattheis, Phys. Status Solidi A **125**, 9 (1991).
[5] J. M. D. Coey, M. Viret, and S. von Molnar, Adv. Phys. **48**, 167 (1999).
[6] G. Van Tendeloo, O. I. Lebedev, and S. Amelinckx, J. Magn. Magn. Mater. **211**, 73 (2000).
[7] A. M. Haghiri-Gosnet *et al.*, J. Appl. Phys. **88**, 4257 (2000).
[8] J. C. Jiang, E. I. Meletis, and K. I. Gnanasekar, Appl. Phys. Lett. **80**, 4831 (2002).
[9] M. Liebmann, A. Schwarz, S. M. Langkat, and R. Wiesendanger, Rev. Sci. Instrum. **73**, 3508 (2002).
[10] See EPAPS Document No. E-PRLTAO-92-082401 for a movie of the magnetization reversal. It shows the MFM data from remanence (0 T) towards saturation (0.6 T) and back to remanence (0 T) together with the hysteresis loop, which has been reconstructed from the evaluation of individual Barkhausen jumps. The cycle consists of 158 MFM images recorded with 5 or 10 mT per frame corresponding to a ramp rate of 0.01 mT/s and 0.02 mT/s, respectively. A direct link to this document may be found in the online article's HTML reference section. The document may also be reached via the EPAPS homepage (http://www.aip.org/pubservs/epaps.html) or from ftp.aip.org in the directory /epaps/. See the EPAPS homepage for more information.
[11] This interpretation of MFM contrast formation is correct as long as magnetic poles are only present at the surface (and not in the volume), the oscillation amplitude of the cantilever is small compared to the domain width, and the magnetic states of neither tip nor sample are changed by each other. All these requirements are fulfilled in the measurements presented.
[12] Y. Wu *et al.*, Appl. Phys. Lett. **75**, 2295 (1999).
[13] Note that the noise level of the measurement has been used as a threshold level to determine a_B. As a consequence, part of the total contrast of each event is hidden below the noise level, i.e., the value of the contrast integral is underestimated. The resulting error is larger for smaller reversed areas. To take this into account an offset of measured area times half of the experimental peak-to-peak noise is added.
[14] A. Hubert and R. Schäfer, in *Magnetic Domains: The Analysis of Magnetic Microstructures* (Springer-Verlag, Berlin, Heidelberg, 1998), p. 80.
[15] According to the molecular field theory, $A = nJ_{ex}S2/a$, where $S = 3/2$ is the manganese spin, $n = 1$ is the number of manganese atoms per unit cell, and $a =$ 389 pm is the lattice constant. The exchange integral J_{ex} can be determined via the Curie temperature $T_C =$ 325 K and the coordination number $z = 6$ (cubic symmetry) using $J_{ex} = 3k_BT_C/2zS(S + 1)$, where k_B is the Boltzmann constant.
[16] P. Bak, C. Tang, and K. Wiesenfeld, Phys. Rev. Lett. **59**, 381 (1987).
[17] J. P. Sethna, K. A. Dahmen, and C. R. Myers, Nature (London) **410**, 242 (2002).
[18] P. J. Cote and L. V. Meisel, Phys. Rev. Lett. **67**, 1334 (1991).
[19] O. Perkovic, K. Dahmen, and J. P. Sethna, Phys. Rev. Lett. **75**, 4528 (1995).
[20] B. Allessandro, C. Beatrice, G. Bertotti, and A. Motorsi, J. Appl. Phys. **68**, 2901 (1990).
[21] S. Zapperi, P. Cizeau, G. Durin, and H. E. Stanley, Phys. Rev. B **58**, 6353 (1998).
[22] D. H. Kim, S. B. Choe, and S. C. Shin, Phys. Rev. Lett. **90**, 087203 (2003).
[23] J. M. Gonzalez, O. A. Chubykalo, and J. Gonzalez, Phys. Rev. B **55**, 921 (1997).
[24] J. S. Urbach, R. C. Madison, and J. T. Markert, Phys. Rev. Lett. **75**, 276 (1995).
[25] L. P. Kadanoff, S. R. Nagel, L. Wu, and S. M. Zhou, Phys. Rev. A **39**, 6524 (1989).